Optical and mechanical design of the Antarctic Submillimeter Telescope and Remote Observatory

Antony A. Stark[a)]
Smithsonian Astrophysical Observatory, 60 Garden Street, Cambridge, Massachusetts 02138

Richard A. Chamberlin and James G. Ingalls
Boston University, Department of Astronomy, 725 Commonwealth Avenue, Boston, Massachusetts 02215

Jingquan Cheng
National Radio Astronomy Observatory, 949 North Cherry Avenue, Tucson, Arizona 85721

Gregory Wright
Bell Laboratories, Crawford Hill, Holmdel, New Jersey 07733

(Received 1 August 1996; accepted for publication 5 February 1997)

Antarctic Submillimeter Telescope and Remote Observatory (AST/RO), a 1.7 m diameter telescope for astronomy and aeronomy studies at wavelengths between 200 and 3000 μm, was installed at the South Pole during the 1994–95 Austral summer. The optical design is Gregorian, offset in both azimuth and elevation, with the exit pupil at the chopping tertiary mirror: this arrangement provides for consistent illumination of the primary mirror even when the beam is thrown one degree or more on the sky. Aberrations are minimized by the choice of secondary mirror offset angle. Alignment is accomplished by mechanical means. There is a Coudé focus in a warm, spacious receiver room and also a Nasmyth focus. Both the elevation and azimuth axes are driven by two pinion gears with opposed torques to eliminate backlash. The encoders are unusually robust but have high friction, necessitating a stiff coupling. The azimuth limit switch scheme permits 1.5 rotations, but the switches will operate under extreme conditions with no single point of failure. The instrument is now operational with four heterodyne receivers and three acousto-optical spectrometers. © *1997 American Institute of Physics.* [S0034-6748(97)02805-0]

I. INTRODUCTION

The Antarctic Submillimeter Telescope and Remote Observatory became operational in January 1995 at the United States National Science Foundation Amundsen-Scott South Pole Station.[1,2] The observatory will carry out programs in astronomy and aeronomy, using a 1.7-m-diam submillimeter-wave antenna. The immediate scientific goals of this instrument are heterodyne spectroscopy of galactic atomic and molecular clouds and molecular lines in the earth's stratosphere at wavelengths near 600 μm, but the antenna was designed to be a general-purpose instrument for the millimeter, submillimeter, and far-infrared. The South Pole is the best ground-based observatory site for these wavelengths, because the cold climate dessicates the atmosphere,[3,4] and water vapor is the dominant source of atmospheric opacity at submillimeter wavelengths.

The design criteria combine logistical and site exigencies with the optimization of the instrument as a submillimeter-wave telescope:

(1) all systems must operate reliably in the South Pole environment (see Table I);
(2) on-site assembly and alignment is minimal;
(3) all components must fit into shipping containers less than 2.4 m in height and width (to fit in the cargo bay of an LC130 aircraft);
(4) the telescope is fully steerable and slews at $2° \ s^{-1}$ or faster;
(5) the beam can be chopped a degree in cross-elevation at a 10 Hz rate;
(6) several receiver packages can be mounted simultaneously;
(7) the field-of-view is large enough to accommodate array detectors (the focal plane should contain hundreds of diffraction-limited resolution elements that have acceptably small aberrations);
(8) the beam efficiency is maximized and spillover minimized;
(9) the beam is diffraction-limited and the beam quality is high for wavelengths as short as $\lambda 200$ μm (surface accuracy better than 10 μm);
(10) pointing accuracy must be within 1/10th beam at $\lambda 200$ μm (3 s of arc);
(11) operation is mostly automatic.

Aside from extreme cold and wind-driven ice crystals, the South Pole is a benign environment for telescopes. The highest recorded wind speed in nearly 40 years of weather station operation is only 24 m/s.[5] Other problems often encountered in telescope operations, such as wet conditions, rapid temperature variations, and insect swarms, do not occur at the South Pole. This article describes the optical and mechanical design of the AST/RO instrument. The optical design, described in Sec. II, is a novel type of offset Gregorian, with the tertiary mirror located at the exit pupil of the instrument. The method by which these optics are made to track astronomical objects in the Polar environment is described in Sec. III.

[a)]Electronic mail: aas@cfa.harvard.edu

 0034-6748/97/68(5)/2200/14/$10.00

TABLE I. Physical environment of the AST/RO telescope.

Altitude	2847 m
Latitude	W 45°53′
Longitude	S 89°59′40″
Average pressure[a]	680 mb
Minimum temperature[a]	−82 °C
Maximum temperature[a]	−14 °C
Average temperature[a]	−49 °C
Average wind speed[a]	5.8 m s^{-1}
Maximum wind speed[a]	24 m s^{-1}
Median water vapor column in summer[b]	0.47 mm PWV
Median water vapor column in winter[b]	0.25 mm PWV
Median observed zenith transmission at 609 μm Wavelength in winter[b]	0.50
Median calculated zenith transmission at 350 μm Wavelength in winter[c]	0.76

[a]Schwerdtfeger (Ref. 5).
[b]Chamberlin *et al.* (Ref. 4).
[c]Bally (Ref. 3).

II. OPTICAL DESIGN

AST/RO is a fully steerable, offset Gregorian telescope with a tertiary chopper mirror at the exit pupil and a four-mirror Coudé arrangement. Figure 1 is a schematic of the optical design. The primary mirror is an offset section of a paraboloid. The secondary mirror is a section of a prolate spheroid. The tertiary and quaternary mirrors are flat. The tertiary mirror is located at the exit pupil and also serves to direct the beam along the elevation axis. The quaternary mirror is at the intersection of the elevation and azimuth axes, and directs the beam through a 140-mm-diam hole in the azimuth axis bearing and encoder to the Coudé room below. If the quaternary mirror is removed, the beam passes through a 0.2 m hole in the elevation bearing to a Nasmyth focus platform.

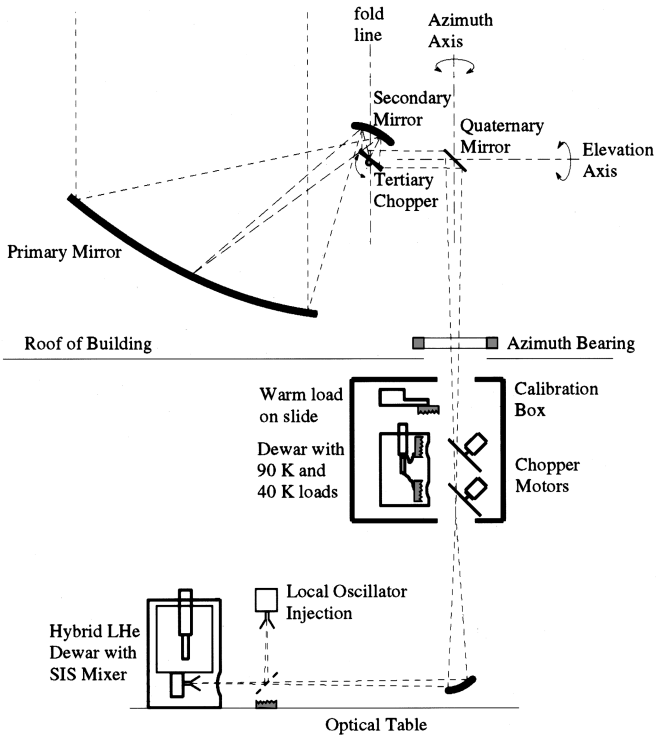

FIG. 1. Schematic of the AST/RO optical system. For purposes of representation, the beam path has been flattened and the reader should imagine that the primary and secondary mirrors are rotated by 90° out of the plane of the page around the vertical ''fold line.'' Note that rays diverging from a point on the primary mirror reconverge at the chopping tertiary mirror, since the tertiary is at the exit pupil of the instrument. The tertiary and quaternary mirrors are flat. The calibration loads are in a Dewar to the side of the Coudé beam entering along the azimuth axis. The ambient temperature load is on a linear actuator and can slide in front of the sky port. Motorized chopper mirrors switch the receiver beam from the cooled loads to the sky or to the ambient temperature load.

Avoidance of internal reflections is important to the design of a submillimeter-wave single-dish telescope like AST/RO. Any receiver or detector placed at the focus of the instrument will necessarily launch into the telescope some amount of submillimeter-wave power in the band of interest. If there is a reflection in the system, for example at the secondary mirror some 3 m distant, then a resonant cavity is formed whose modes are spaced at roughly 50 MHz intervals, and spurious features at those intervals will appear in the spectrometer whenever there is a shift in power level or small change in the cavity. Submillimeter-wave spectrometers cover more than 1 GHz of bandwidth, and a 50 MHz spurious feature can masquerade as a typical astronomical or atmospheric line with a Doppler broadening of $\sim$30 km s^{-1}. All of the optics in AST/RO are offset so that internal reflections and resonances do not occur.

Like all radio telescopes, AST/RO has a diffraction-limited beam, and diffraction effects will tend to dominate the classical optical aberrations such as coma and astigmatism. Moving outward from the center of the sagittal image surface, aberrational blur is significant only when it becomes comparable to diffraction blur. Dragone[6] has shown that if the offset angles in an offset Cassegrain or Gregorian antenna are chosen correctly, then aberrations and cross-polarization effects in an offset antenna are the same as those in a conventional on-axis antenna with the same diameter and focal length. The beam efficiency and sidelobe levels in the off-axis antenna are better than those in the on-axis antenna, because in the on-axis design there will be diffraction, reflection, and blockage from the secondary mirror and its supports. An off-axis Cassegrain or Gregorian antenna with correctly chosen offset angles will always be optically superior in the diffraction-limited regime to a similar on-axis configuration, although the off-axis antenna may be mechanically more complex and expensive.

A. Beam chopper considerations

Gregorian telescopes have a small advantage in aberration and image curvature over Cassegrain telescopes of the same diameter and focal length, but are less commonly built because the primary-to-secondary distance is larger and for on-axis Gregorian designs the aperture blockage is greater. Aperture blockage is not a problem for off-axis configurations. Larger primary-to-secondary distance can be a structural disadvantage, especially for large instruments. Gregorian telescopes do, however, have a significant feature which Cassegrain telescopes do not: Gregorian telescopes have a real exit pupil, a position along the beam path where the secondary forms an image of the primary mirror surface. In AST/RO, the exit pupil is the location of the flat tertiary

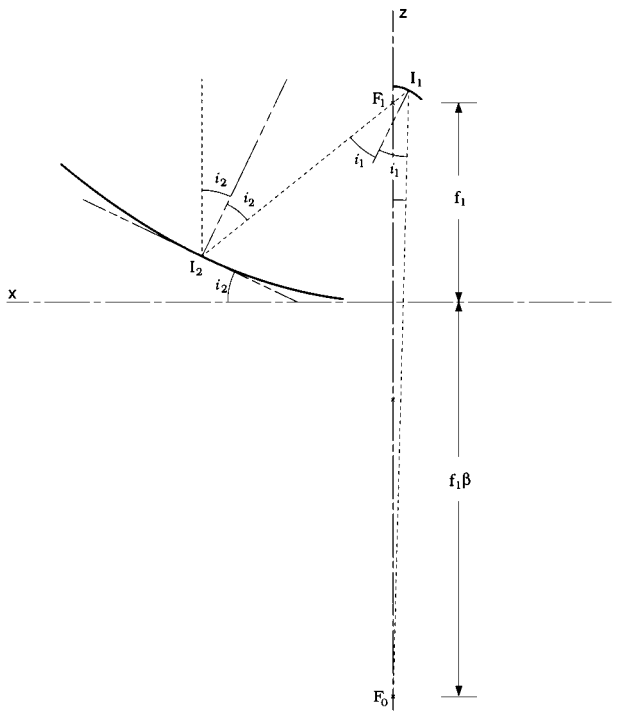

FIG. 2. Scale drawing of the primary mirror and long focal length secondary mirror. The line F_1F_0 is the axis of symmetry of the paraboloid of which the primary is a section and the prolate spheroid of which the secondary is a section.

mirror, a motor-driven, rotating chopper, as shown in Fig. 1. This location for the chopper is crucial to its operation. All rays which strike the primary mirror (which is to say, all rays admitted by the telescope system) also strike the chopper mirror. Furthermore, changing the angle of the chopper mirror only changes the direction of the rays at the primary mirror, not their position. Imagine time-reversed radiation propagating through the telescope, so that the receiver acts as a transmitter. The beam launched by the receiver illuminates the chopper mirror. Since the chopper mirror is at the exit pupil, this illumination pattern maps onto the primary mirror with a mapping which is independent of chopper mirror angle, so that the illumination pattern does not change as the chopper is rotated. The chopper tilts the phase front of the Gaussian beam striking the primary without changing the power distribution pattern. In forward-time, spillover radiation seen by the receiver does not change significantly as the chopper is rotated.

The position of the exit pupil is not far from the secondary mirror, slightly further from the secondary mirror than the distance to the prime focus (the prime focus is point F_1 in Fig. 2). Tilting the chopper by an angle θ_c results in a beam throw on the sky of

$$\theta_s \simeq 2\frac{(F_1I_1)}{(F_1I_2)} \cdot \theta_c ,$$

where F_1I_1 is the short focal distance of the secondary mirror and F_1I_2 is the focal distance of the primary mirror. Some observing methods require $\theta_s \sim 3°$, while $(F_1I_1)/(F_1I_2) \sim \frac{1}{12}$, so the angle through which the chopper rotates can be fairly large, $\theta_c \sim 18°$. The center of chopper rotation places the chopper mirror at a 45° angle to the beam, turning the central ray through 90°. The chopper must be elongated in order to intercept all of the beam, even when rotated into an orientation where the central ray is turned through an oblique angle; the chopper length must be $\sec(45° + \theta_c)$ larger than its width. If θ_c is large, the mirror must be so long that it will strike the secondary mirror when turned the other way from the central 45° position. For a given primary focal length F_1I_2, the criterion that the the chop angle on the sky, θ_s be as large as possible (while the chopper mirror is at the exit pupil and the chopper mirror is large enough not to vignette the beam but small enough not to hit the secondary) sets the focal length of the secondary mirror F_1I_1. There is a range of acceptable solutions near $(F_1I_1)/(F_1I_2) \simeq \frac{1}{12}$, and the maximum beam throw is $\theta_s \sim 3°$. The usable beam throw may be smaller than this because of curvature of field, as will be discussed below.

B. Optics geometry

Although AST/RO itself is offset in both azimuth and elevation, the primary and secondary mirrors are bilaterally symmetric about a vertical plane, and Fig. 2 shows the intersection of the mirror surfaces with the plane of symmetry. The Gregorian secondary is a section of a prolate spheroid with focii at F_0 and F_1. The paraboloidal primary has a focus at F_1. The central ray is a short dashed line. In this figure the telescope is looking toward the zenith, along the z axis. The coordinate system, (x,y,z) has its origin the vertex of the primary mirror paraboloid, and the focus of the paraboloid is at (0, 0, 1200 mm), so the surface of the primary mirror satisfies the equation

$$z = \frac{x^2 + y^2}{4f_i}, \tag{2.1}$$

where $f_1 = 1200$ mm. The primary mirror is a piece of this surface bounded by a cylinder 1700 mm in diameter, with its axis parallel to z at $x = 1150$, $y = 0$. The central ray follows this axis from $z = \infty$ until it intercepts the center of the primary mirror at (1150 mm, 0, 275.521 mm), where it reflects at an angle of incidence $i_2 = 25.^{\circ}60$, through Focus 1 at (0, 0, 1200 mm), to the center of the secondary at (−94.89 mm, 0, 1276.43 mm). The focal ratio at the prime focus is 0.779. Following the secondary mirror are a flat tertiary (the chopper) which directs the beam along the elevation axis, and a flat quaternary which directs the beam down the azimuth axis. From the secondary to the chopper is 127.8 mm, from the chopper to the quaternary is 389.6 mm, and from the quaternary to the optics table is 3942.6 mm. The geometrical Coudé focus is 800 mm above the optics table; the 492 GHz beam waist is 155 mm closer to the secondary mirror because of finite-wavelength effects.

There are two secondary mirrors intended to be used with instruments at the Coudé focus and Nasmyth focus. First consider the longer focal length Coudé mirror. Its surface is determined by four criteria:

(1) the mirror has two focii, one coincident with the primary mirror;

(2) the line segment connecting the two focii is aligned with the z axis;
(3) the vertex-to-focus distance is exactly 1/12th that of the primary, i.e., 100 mm (this is the condition for maximum chopper throw on the sky, cf. Sec. I A);
(4) the distance from the mirror center to the second focus is 3660 mm, in order to place the geometric focus of the secondary 800 mm above the optics table in the Coudé room.

The surface of this table is 4460 mm from the center of the secondary along the optical path. These conditions are satisfied by an ellipsoid whose equation is

$$\left(\frac{z-z_c}{a}\right)^2+\left(\frac{x}{b}\right)^2+\left(\frac{y}{b}\right)^2=1, \tag{2.2}$$

where $z_c=-591.099$ mm, $a=1891.099$ mm, $b=606.811$ mm.

The input phase front radius of the Coudé focus secondary is therefore $R_1=122.20$ mm, the output phase front radius is $R_2=3660$ mm, and half the angle through which the beam is turned is $i_1=24.^{\circ}86$, according to the Gaussian beam formalism of Chu.[6]

The Nasmyth secondary is also determined by four criteria:

(1) it has two focii, one coincident with the primary mirror;
(2) the second focus lies on the central ray determined by the ''long'' mirror, so that the tertiary mirror does not have to be realigned when the secondary mirror is changed;
(3) the second focus is 1016 mm from the focus of the long mirror—this is the difference in path lengths between the Coudé focus and the Nasmyth focus;
(4) one point on the short mirror's surface is coincident with a point on the long mirror's surface—this point is chosen to be point of intersection of the surface with the ray closest to the z axis at (-24.98 mm, 0, 1298.38 mm).

The choice of this point of intersection results in the two surfaces lying close together over most of the area of the secondary mirror. These conditions are satisfied by an ellipsoid with semimajor axis $a=570.01$ mm semiminor axis $b=321.25$ mm, and tilted by $4.^{\circ}1742$ with respect to the z axis.

C. Aberrations

Dragone[7] has shown that for an offset Gregorian or Cassegrain system with offset angles i_1 and i_2, the aberration function is equivalent to that of a single-reflector prime-focus paraboloid with offset angle i_0, where

$$\tan i_0=(1-M)\tan i_1+M\tan i_2, \tag{2.3}$$

and focal length

$$f_0=Mf_1, \tag{2.4}$$

where $M=(F_0I_1)/(F_1I_1)$ is the magnification of the secondary. For the AST/RO Coudé focus, $M=-30.03$, and $f_0=44{,}310$ mm. Aberrations are minimized if $\tan i_0=0$. For AST/RO, $i_0=-0.^{\circ}7$, sufficiently small that the most significant classical aberration is coma, and even coma is very small because the magnification is high. The value of i_1 was chosen so that the point F_0 lies on the z axis, which is the line of rotational symmetry for the surfaces of which the primary and secondary are sections; AST/RO has the geometry of an on-axis telescope where only an off axis bundle of rays is admitted to the instrument. Choosing i_1 this way is equivalent to Dragone's minimum aberration condition $\tan i_0=0$ in the limiting case of large secondary magnification $|M|$.

What actually limits the usable field-of-view for AST/RO is field curvature: all aberrations are smaller than the diffraction-limited blur, even in the highly curved outer parts of the surface of best images. This surface is essentially the same as that of the equivalent on-axis Gregorian of which AST/RO is a piece. The curvature constant of the surface of best images is therefore:

$$\kappa_m=\frac{2}{R}\left(\frac{(m^2-2)(m-\beta)+m(m+1)}{m^2(1+\beta)}\right), \tag{2.5}$$

where $m=36.8$ is the on-axis secondary magnification, $\beta=1.98$ is the scaleless back-focal length, and $R=2f_1=2400$ mm is the curvature of the primary at the vertex.[8] For the Coudé secondary, where $m=-36.8$ and $\beta=1.98$, $\kappa_m=-0.01$ mm^{-1}, giving a usable field-of-view about 100 mm diameter or 8 arcmin on the sky. For the Nasmyth secondary, where $m=-10.5$ and $\beta=0.13$, $\kappa_m=-0.007$ mm^{-1}, giving a usable field-of-view about 142 mm in diameter or 40 arcmin on the sky.

D. Gaussian beam analysis

A Gaussian beam analysis of the optics was done to ensure that the beam could propagate through the telescope without excessive loss and to match the receiver beams to the antenna.[6,9] The Coudé focus design was optimized for operation at λ610 μm, but is suitable for wavelengths as long as λ1.2 mm. Table II gives the parameters of the focusing mirrors of the AST/RO telescope. The radii R_1 and R_2 are the distances along the central ray to foci of the mirror.

The Gaussian beam radii for the Coudé focus beams at 0.61 and 1.2 mm wavelength are given in Table III. (The Gaussian beam radius is the radius of the e^{-1} amplitude

TABLE II. Mirror parameters.

	R_1	R_2
Primary	∞	1475.52 mm
Coudé secondary	122.20 mm	3660.00 mm
Nasmyth secondary	220.98 mm	1300.00 mm

TABLE III. Gaussian beam radii (Coudé focus).

	λ = 0.61 mm	λ = 1.2 mm
Primary	698.78 mm	701.81 mm
Prime focus	0.41 mm	0.87 mm
Calibration load	27.10 mm	35.30 mm
Coudé focus	11.99 mm	23.28 mm
Optical table	19.68 mm	34.04 mm

TABLE IV. Gaussian beam radii (Nasmyth focus).

	$\lambda = 1.2$ mm	$\lambda = 3$ mm
Primary	498.77 mm	457.37 mm
Prime focus	1.13 mm	2.82 mm
Nasmyth focus	6.92 mm	16.77 mm

point.) The design wavelength is $\lambda = 0.61$ mm, and the radii for $\lambda 1.2$ mm assume that the focusing mirrors are left in their optimum $\lambda 610$ μm positions. The primary illumination tapers to -15 dB at the edge at the design wavelength. All apertures are at least twice the diameter of the $\lambda 1.2$ mm Gaussian beam. The Coudé focus was placed midway between the optical table on which the receivers are mounted and the calibration load dewar which is suspended from the underside of the azimuth bearing structure. This is a compromise between having a small beam size on the optical table, and minimizing the size of the calibration loads and choppers. The last third and fifth entries in Table III give the beam radius on the calibration load and at the first mirror on the optical table, respectively. A somewhat smaller beam on the optical table was favored to reduce the size of the quasi-optical sideband rejection filter and local oscillator injection optics.

The Nasmyth focus is designed for continuum observations at 3 mm wavelength (Table IV). It can also be used at shorter wavelengths, for example, $\lambda 1.2$ mm. As before, the table shows the Gaussian beam radii at the off-design wavelength assuming that the mirrors remain in their optimum design wavelength positions. At $\lambda 3$ mm, the primary illumination tapers to -30 dB at the edge. This reduces the amount of power diffracted into the beam from the surroundings, at the expense of increasing the beam size. The beam size full width half-maximum (FWHM) at 3 mm is 8.9 ft.

E. Primary-secondary alignment

The mount of the secondary mirror of AST/RO is designed so that the mirror may be translated along three orthogonal axes by approximately 2 cm. This limited range of motion is sufficient to orient the secondary mirror with respect to the tertiary and subsequent mirrors. The primary mirror is then aligned with respect to the secondary. The primary-secondary alignment is critical, because these are highly curved elements with low f/D ratios; the tertiary and quaternary mirrors are flat, so their alignment does not affect beam quality. The primary mirror is kinematically mounted to the steel mirror cell by three pairs of struts. The struts attach at six pivot points to the steel mirror cell. Each strut pair meets at a pivot point at the back of the mirror (a ''hexapod'' arrangement). The struts incorporate a turnbuckle which may be rotated to lengthen or shorten the strut, and thereby change the orientation of the primary. The mount is kinematic: the six struts constrain the mirror in precisely all six degrees of freedom, so the mirror is held rigidly in place, but the mount cannot create stresses internal to the mirror. Since the struts motions are not orthogonal, however, proper orientation of the primary is not straightforward.

Both the primary and secondary reflectors have been fabricated with four polished and hardened steel reference balls mounted with roughly equal spacing around the edge of the mirror. The balls have precise diameters, and the positions of the balls with respect to the mirror surface were measured at the time each mirror was measured in the shop after fabrication. The positions of the centers of the balls are therefore accurately known with respect to the best-fit curve for the mirror surface. The 16 distances between each of the primary balls and each of the secondary balls can then be calculated for a perfectly aligned system. A micrometer may be used to measure the distances and align the two mirrors. Since the secondary is kept fixed, the coordinate system of the secondary is taken to be the coordinate system of the perfectly aligned system. A computer program was written to take between six and 16 primary-to-secondary distance measurements, with errors, and find the actual positions of the primary mirror balls with respect to this coordinate system. The program uses a nonlinear least-squares method, to fit for the three rotations and three translations of the primary mirror which best recover the measured distances. An initial set of measurements of the mounting strut lengths enables the program to estimate the position of the primary mirror cell in the secondary mirror coordinate system. The program then calculates the number of turns of the strut turnbuckles to bring the primary into alignment with the secondary.

Using a tubular inside micrometer, measurements were made of a subset of the 16 possible primary-secondary ball distances. The measurements were accurate to within 40 μm. The computer program was used to reorient the primary mirror, and the measurements were made again. Initially, the primary-secondary ball distances deviated from perfect alignment with an rms of approximately 3 mm. After eight iterations of this procedure, the distances deviated from the calculated alignment position with an rms of 220 ± 90 μm, less than 1 wavelength at 492 GHz.

III. MECHANICAL DESIGN

The antenna is arranged so that temperature sensitive components such as the drive motors, encoders, cables, and bearings are on the innermost layer of the telescope and are surrounded by a steel semimonocoque structural shell. The steel is covered with insulating foam, which in turn is covered with an aluminum skin. At the rotary joints, the aluminum layer is sealed against the intrusion of ice crystals by brush seals. The telescope sits on top of a building, and the base of the telescope is sealed to the roof with a silicone rubber skirt. The weight of the telescope is borne by a steel tower which extends through the building but is not in structural contact with it. The base of the telescope is approximately 7 m above the surface, well above most blowing ice crystals. The entire building is elevated on steel supports by 4 m above the snow surface, in order to minimize snow drifts.

The building has six rooms, used for telescope control, laboratory space, and storage. The largest room, $4.8\ \text{m} \times 4.8\ \text{m}$ in floor area, is directly under the telescope and serves as a Coudé room. The interior of the antenna structure is connected to the interior volume of this room

through an 0.8-m-diam hole in the azimuth bearing and a 1.2 m×1.3 m hole through the roof and telescope support tower. Heated (20 °C) air from the building flows up through the interior of the antenna structure, keeping it warm. Most of the warm air escapes through a 100-mm-diam hole at the point where the submillimeter-wave beam enters the telescope structure. This point coincides roughly with the prime focus, between the primary and secondary mirrors. There are no windows or other dielectric surfaces in the submillimeter-wave beam, except at the entrances to vacuum Dewars.

The primary mirror consists of a single 1.7 m×1.9 m panel, mounted kinematically from three points on its back. The panel is a sandwich of aluminum honeycomb between two carbon fiber-epoxy skins with a vacuum-sputtered aluminum surface having a surface roughness of 6 μm and an rms figure of about 9 μm.[10] The panel size is near maximal for a panel of a few microns surface accuracy made with these materials. This is also a size which fits in the cargo bay of the LC-130 aircraft used to supply the South Pole. The 1.7 m aperture yields a beamsize of 96 arc sec(λ/600 μm), a beam arc sec which is large enough to allow large-scale mapping programs, yet small enough to map distant clouds in the galaxy and to just resolve hundreds of external galaxies, a good aperture size for a survey instrument. The beam is not small enough, however, to resolve distant galaxies or to study protostellar regions in any detail.

Because the primary mirror is not large, the telescope structure is also relatively small. The total volume of the cryogenic receivers is comparable to the volume of the telescope itself, and the receivers work best in a nontilting, warm environment where the cryogenics can easily be serviced. The Coudé arrangement allows for convenient mounting and simultaneous operation of several receivers. An aluminum truss suspended from the telescope support tower into the receiver room holds four 0.7 m square optical table ''pallets'' at a convenient height above the floor, and each of these is used to mount one receiver. The receivers are thus mechanically connected to the telescope and telescope support tower and not to the floor of the receiver room, but they sit on a horizontal surface at benchtop level in a laboratory environment. Also suspended from the bottom of the telescope, at the height of the Coudé room ceiling, is a calibration box consisting of a dewar with 90 and 40 K cold calibration loads, a room-temperature load, and computer-operated movable mirrors for directing the submillimeter-wave beam into the loads. The azimuth structure above roof level incorporates a Nasmyth focus platform which rotates with the telescope.

Optimizing the optics with a tertiary chopper on the elevation axis requires that the primary mirror be cantilevered away from the elevation axis: this is accomplished with a truss of Invar™ rods which hold the primary-to-secondary distance invariant with temperature. The Invar rods are screwed at one end to steel rings attached to the bearings, and at the other end to the steel primary mirror cell to which are connected the primary mirror struts.

There are two elevation bearings and one azimuth bearing. The azimuth bearing and one of the elevation bearings are fully constrained and preloaded large diameter bearings with integral gears. This type of bearing was developed for heavy machinery like excavators and cranes; recent improvements in machining techniques have allowed such bearings to be made with sufficient accuracy for astronomical use. For example, the instantaneous rotation axis of the azimuth bearing wobbles by roughly 30 arc sec in the course of a rotation, but the wobble pattern is reproducible at the sub-arcsecond level, and the effects can therefore be accurately corrected in the computer control of the pointing. The second elevation bearing is a spherical roller bearing, and serves only to support half the weight of the elevation structure without imposing additional constraints. All of the bearings and motors are packed with a low-temperature, high-pressure grease consisting of molybdenum disulphide in a synthetic carrier. This grease works well at temperatures down to -75 °C.

The telescope as shown in Fig. 3 disassembles into three large pieces for shipment. The primary mirror is removed from the mirror cell. The eight Invar truss rods connecting the mirror cell to the elevation structure attach with a single large screw at each end; when these are removed the remainder of the elevation structure can be folded down to reduce the overall height of the combined elevation/azimuth/base structure to about 2.1 m.

A. Drive system

External gears are cut into the outer rings of the large-diameter azimuth and elevation bearings. Pointing the telescope involves positioning these gears with an accuracy of about 3 arc sec; taking into account wind loading, the inertia of the telescope, and friction. Wind loading dominates the torque requirements: a 25 m s^{-1} wind could create torques of 1000 N m on the axes; the drives are capable of delivering this torque and as a result can accelerate the telescope very quickly under normal wind conditions. On the other hand, it is not desirable to drive the telescope axes at a speed greater than 2 rpm in slew mode, and tracking of astronomical sources requires accurate position and velocity control at axis speeds of about 2×10^{-4} rpm. Low speed, high-torque operation is achieved by geared down electric motors. A speed range of 10 000:1 between slew and tracking speeds, and accurate velocity control at low speeds is achieved through use of dc servo motors designed for low-speed operation. Brushed dc motors can be operated manually using a simple battery-powered circuit during telescope construction and under emergency conditions.

Each axis gear is driven by two pinions, and each pinion is driven by a gearhead/motor/tachometer/brake (GMTB) package, so that four motors operate the telescope. All of the GMTB packages are identical, and the two drives are identical except for the gears on the axis bearings themselves. Drive parameters are summarized in Table V.

The total gear ratio between the motor and the elevation axis is $N_E = 871\frac{3}{7}$, and the total ratio between the motor and the azimuth axis is $N_A = 1685\frac{5}{7}$. The motors have a rated torque of $T_M = 0.6$ N m; they can produce this torque indefinitely at any rated speed without thermal overload. The torque available at the antenna axes are

$$T_E = 2E_G N_E T_M = 850 \text{ N m}$$

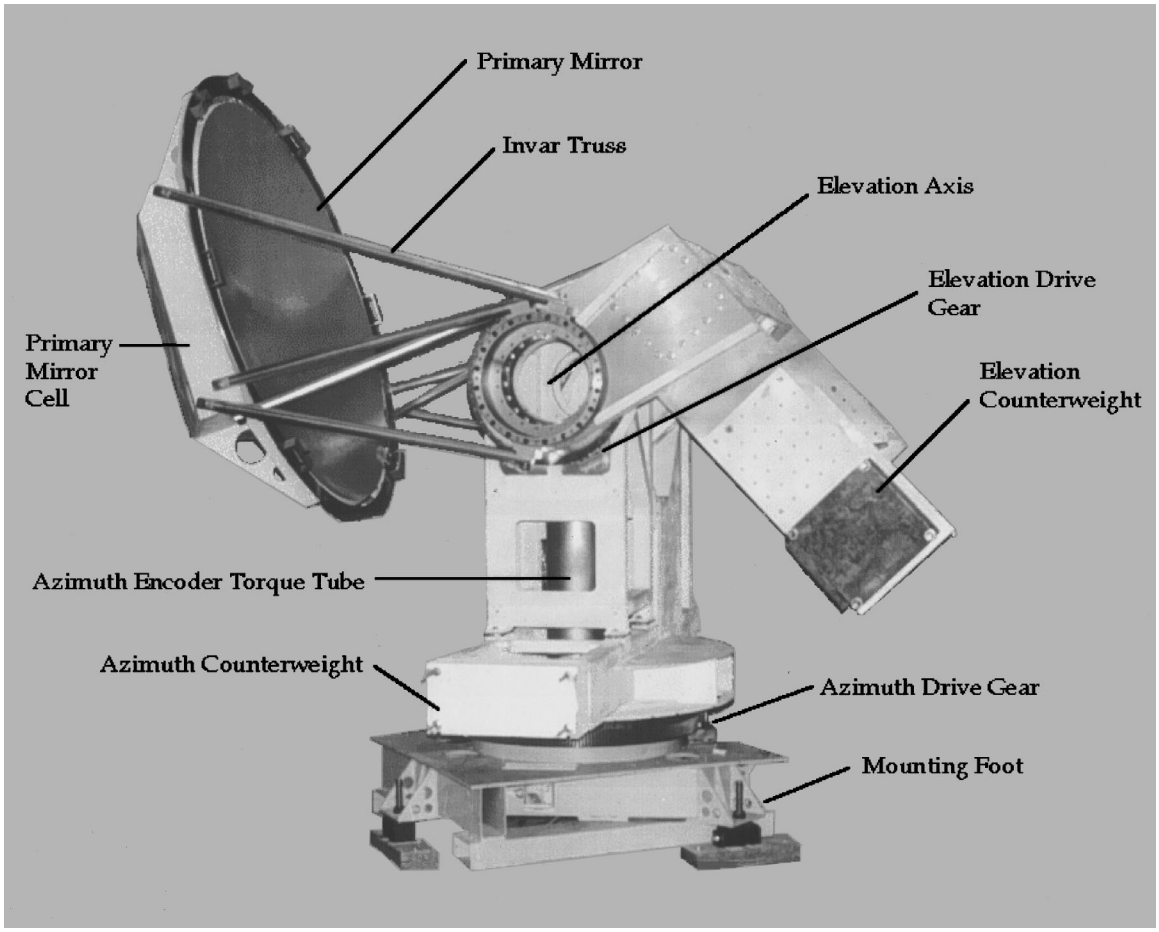

FIG. 3. The AST/RO telescope, as first assembled at the Boston University Scientific Instrument Facility in December 1992. The outer insulation and aluminum protective skin had not yet been installed.

and

$$T_A = 2E_G N_A T_M = 1638 \text{ N m}.$$

These are the torques that can be delivered to the axes indefinitely without exceeding the system ratings in any way. The motors, however, are capable of much higher torques for short periods of time. The rated torque is determined by the cooling rate of the rotor. If the continuous stall current $I_M = 7.5$ A is supplied to the motor, it will produce the rated torque of $T_M = 0.6$ N m, and will warm to a steady state where heat diffuses out of the rotor at the same rate it is produced. Currents several times larger than I_M, if applied for short periods of time (about 0.5 s—long enough to accelerate to full speed), will not overheat the rotor and during these periods the motor will produce much more torque. The servo system is designed to provide short periods of high current operation. The drive system is then limited by the gearhead, which will begin to experience increased wear and possible damage. Damage to the gearhead from excessive static torque can be avoided by limiting the current at the motor drive amplifiers to less than 24 A, but excess dynamic torque can still be a problem if the motor current is changed too rapidly.

The antenna moments of inertia reflected through the gearing are about eight times larger than the moments of one GMTB package. The motor speeds are limited to 1500 rpm, so slew speeds on the axes are

$$V_E = 1500 \text{ rpm}/N_E = 1.7 \text{ rpm} = 10.3°/\text{s}$$

and

$$V_A = 1500 \text{ rpm}/N_A = 0.9 \text{ rpm} = 5.3°/\text{s}.$$

At rated torque, the drives will reach this speed within 200 ms. At the beginning of a slew and the end of a slew, the drives will require this time to accelerate the antenna. The antenna will be moving at maximum slew velocity for the remainder of the time. The shortest slew during which the antenna reaches maximum velocity before decelerating is about 1°.

The reason for having two motors on each axis is that the large gear and pinion gear have a backlash which is much larger than the pointing specification: $2B_P/D_E = 50$ arc sec$\gg$3 arc sec. High accuracy is required only while tracking at low speed, and in that mode the two motors on each axis are commanded to have opposite torques in order to take up the backlash and windup in the gearing. The total torque on one axis is the sum of the torques of the two GMTE sets, and the two torques can add or partly cancel, depending on the mode of operation.

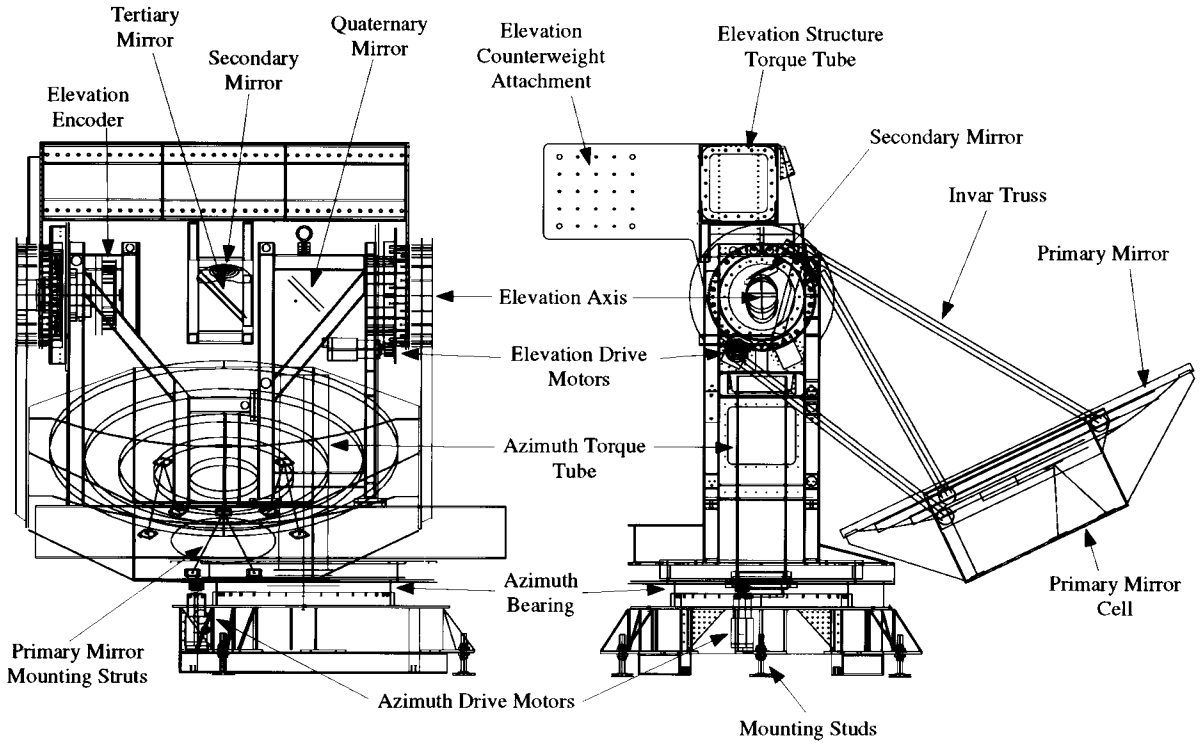

FIG. 4. Mechanical drawing of the AST/RO antenna. Note that the instrument is offset in both azimuth and elevation. As shown, the antenna is pointed at the zenith. Two elements of the Invar truss that connect the bottom outside corners of the primary mirror cell to the top center of the elevation torque tube are not shown. The rotating part of the elevation bearings are toward the outside of the structure. The square steel tubing shown in the azimuth structure is welded to a skin of steel sheet metal.

One potential problem with this system is that the motors and the antenna, considered as three bodies, will oscillate with respect to each other through the springiness of the gears. Consider the model of the system shown in Fig. 5. The moment of inertia and damping of the telescope are evaluated as reflected through the gearing, and static friction is ignored. The equations of motion of the system are

$$J_0 \frac{d^2\theta_0}{dt^2} = -k_1(\theta_0-\theta_1)-k_2(\theta_0-\theta_1)-D_0\frac{d\theta_0}{dt}, \quad (3.1)$$

$$J_1 \frac{d^2\theta_1}{dt^2} = -k_1(\theta_1-\theta_0)-D_1\frac{d\theta_1}{dt}+T_1, \quad (3.2)$$

$$J_2 \frac{d^2\theta_2}{dt^2} = -k_2(\theta_2-\theta_0)-D_2\frac{d\theta_2}{dt}+T_2. \quad (3.3)$$

The antenna position variable θ_0 will exhibit a variety of behaviors depending on the time history of the torques input by the motors, T_1 and T_2. The generalized response of θ_0 to input torques can be approached through the transfer function relating θ_0 to T_1 and T_2. Take the Laplace transform[11] of Eqs. (3.1), (3.2), and (3.3):

$$J_0 s^2\theta_0(s)+k_1\theta_0(s)-k_1\theta_1(s)+k_2\theta_0(s)-k_2\theta_2(s) + D_0 s\theta_0(s)=0, \quad (3.4)$$

$$J_1 s^2\theta_1(s)+k_1\theta_1(s)-k_1\theta_0(s)+D_1 s\theta_1(s)=T_1(s), \quad (3.5)$$

$$J_2 s^2\theta_2(s)+k_2\theta_2(s)-k_2\theta_0(s)+D_2 s\theta_2(s)=T_2(s). \quad (3.6)$$

Define three quadratic function of s:

$$Q_0 \equiv J_0 s^2+D_0 s+k_1+k_2, \quad (3.7)$$

$$Q_1 \equiv J_1 s^2+D_1 s+k_1, \quad (3.8)$$

$$Q_2 \equiv J_2 s^2+D_2 s+k_2. \quad (3.9)$$

Rearranging terms to eliminate $\theta_1(s)$ and $\theta_2(s)$ yields the transfer equation:

$$\theta_0(s)=\frac{k_1Q_2T_1+k_2Q_1T_2}{Q_0Q_1Q_2-k_1^2Q_2-k_2^2Q_1}.$$

The behavior of this function is governed by its poles, which are roots of the denominator. Since the GMTB sets are essentially identical, take $k_1=k_2$ and $Q_1(s)=Q_2(s)$, and this sixth order polynomial becomes factorable and analytically solvable. Taking worst-case values of $k_1=K_{mG}/N_G^2 = 790$ N m/radian, $D_1=0.175$ N m/radian/s, $D_0=0$, $J_1 = 0.175$ N m s^2, and $J_0=0.735$ N m s^2, the poles of the transfer function are

$$s_1=0, \quad (3.10)$$

$$s_2=(-0.080+10.7i)\ \text{Hz}, \quad (3.11)$$

$$s_3=(-0.080-10.7i)\ \text{Hz}, \quad (3.12)$$

$$s_4=-0.051\ \text{Hz}, \quad (3.13)$$

$$s_5=(-0.054+13.0i)\ \text{Hz}, \quad (3.14)$$

$$s_5=(-0.054-13.0i)\ \text{Hz}, \quad (3.15)$$

TABLE V. Parameters of AST/RO drives.

Moment of inertia, elevation	J_E	1000 N m s^2
Number of teeth on elevation gear	N_{GE}	122
Pitch diameter of elevation gear[a]	D_E	516.5 mm
Static friction, elevation gear[a]	T_{fE}	50 N m
Moment of inertia, azimuth	J_A	5000 N m s^2
Number of teeth on azimuth gear	N_{GA}	236
Pitch diameter of azimuth gear[a]	D_A	999 mm
Static friction, azimuth bearing[a]	T_{fA}	100 N m
Number of teeth on pinions	N_P	14
Pitch diameter of pinion	D_P	59.3 mm
Backlash at pinion	B_P	0.1 mm
Rated torque of pinion	T_P	207 N m
Gear ratio of gearhead[b]	N_G	100:1
Rated output torque of gearhead[b]	T_G	87 N m
Ultimate torque of gearhead[b]	T_{uG}	178 N m
Rated overhung load, gearhead bearing[c]	L_G	80 N m
Rated axial load, pinion bearing[c]		2224 N
Efficiency of gearhead[b]	E_G	0.8
Zero-torque output spring constant of gearhead[b]	K_{mG}	4×10^3 N m/radian
Typical output spring constant of gearhead[b]	K_G	2.44×10^4 N m/radian
Motor rated torque[c]	T_M	0.6 N m
Motor peak torque[c]	T_{uM}	6.4 N m
Motor continuous stall current[c]	I_M	7.4 A
Motor peak current[c]	I_{uM}	79 A
Motor rated speed[c]	V_M	2000 rpm
Motor peak speed[c]	V_{uM}	4000 rpm
Motor torque constant[c]	K_{tM}	0.08 N m/A
Motor electrical constant[c]	K_{eM}	8.8 V/krpm
Motor terminal resistance[c]	R_{tM}	0.84 Ω
Motor armature resistance[c]	R_{aM}	0.66 Ω
Maximum motor armature inductance[c]	L_{aM}	100 μH
Motor mechanical constant[c]	T_{mM}	2.7×10^{-3} s
Motor electrical constant[c]	T_{eM}	1.4×10^{-4} s
Motor speed constant[c]	K_{sM}	890 rpm/N m
Tachometer output constant[c]	K_{eT}	2.00 V/krpm
Tachometer output impedance[c]	R_{0T}	4 Ω
Brake holding torque[c]	T_B	0.9 N m
Brake voltage[c]	V_B	24 VDC
Brake power[c]	P_B	9 W
GMTB frictional torque[c]	T_{fM}	0.024 N m
GMTB viscous damping[c]	K_{dM}	0.012 N m/krpm
Inertia of GMTB[c]	J_M	1.1×10^{-4} N m s^2
Mass of GMTB[c]	W_M	6.8 kg
Amplifier gain[d]	g_a	1.6 A/V
Amplifier rated current[d]	I_a	±8 A
Amplifier peak current for 0.4 s[d]	I_{ua}	±16 A
Amplifier bandwidth, uncompensated		1 kHz

[a]Rotek, Inc.; Aurora, OH 44202 Specifications for models A8-17E21 (elevation) and R8-35EXX2 (azimuth).
[b]Harmonic drive; 51 Armory St., Wakefield, MA, 01880; specifications for model HDC 5 C cup-type harmonic drive components.
[c]PMI Motion Technologies; 39 Mall Drive, Commack, NY 11724; specifications for model S9M4HI/BRK/S9A4T/H9D-100 gearhead/motor/tachometer/brake package.
[d]PMI; specifications for model VXA-38-8-16.

where s_1 corresponds to the three bodies stationary at some position, s_2 and s_3 correspond to the antenna axis stationary and the two motor rotors oscillating in opposite directions, s_4 corresponds to the entire ensemble slowing to a halt under the viscous drag of the motors, and s_5 and s_6 correspond to an oscillatory mode where both motors move in one direction and the antenna moves in the opposite direction. These solutions show that there are two timescales of interest: an oscillation with a period of about 100 ms$\approx 2\pi(J_0/k_1)^{1/2}$ $\approx 2\pi(J_1/k_1)^{1/2}$, and an exponential decay with a timescale of 20 s$\approx 2\pi J_0/D_1$.

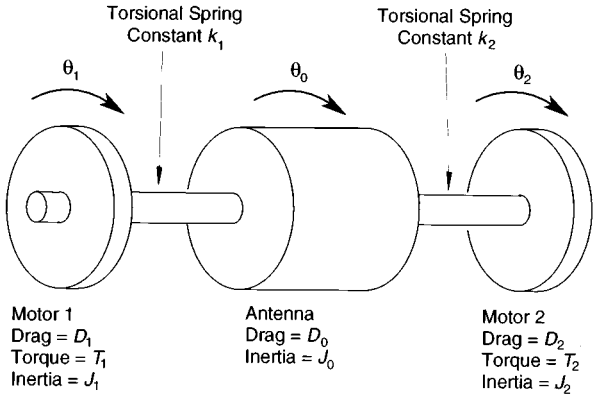

FIG. 5. A simplified model of the two-motor drive system. The model parameters of the motors are those of an equivalent system with no gearing.

Because the simplified analytic analysis above neglects static friction and the viscous drag of the main bearings, the actual exponential decay time is several times shorter than this. The actual oscillation period of the drive system is shorter than 100 ms, because the value of k_1 above is a minimum specification. The harmonic drive gearhead is said to have ''zero backlash,'' but has a low stiffness at low torque and a higher stiffness when the gearing is ''wound up'' at its operating torque level. The stiffness of the gear system is nonlinear, and the spring constant k_1 used above is the minimum value found at zero torque. At a torque level 20% of the rated torque, the spring constant increases by a factor of more than 5. The antibacklash scheme using two motors puts the gearhead in this high spring constant regime, so the oscillation period is less than 50 ms under actual operating conditions.

As shown in Fig. 6, the servo system on each axis has three nested feedback loops. The innermost loop controls the current to each motor. Surrounding this loop is a velocity feedback loop operating from the tachometers in the GMTB sets. Both of these circuits are realized as analog circuits. Outermost is a position loop where the position encoder is read by the computer and compared to the position calculated by the observing program. The antibacklash torque bias is implemented by an offset voltage introduced to the inputs of the current loops.

At tracking speeds, the motors turn at about 0.3 rpm, and the output of the tachometers is about 1 mV. The computer reads the encoder position, and will calculate the desired position (θ_c) and velocity ($d\theta_c/dt$). It will then generate an output voltage on a D/A converter:

$$V_c = g_p(\theta_c - \theta_0) + g_v K_{eT}\left(\frac{d\theta_c}{dt} - \frac{d\theta_1}{dt}\right). \tag{3.16}$$

The computer generated voltage is filtered, and added with an analog circuit to the voltage generated by the tachometers:

$$V_{d1} = g_d K_{eT}\left(\frac{d\theta_2}{dt} - \frac{d\theta_1}{dt}\right). \tag{3.17}$$

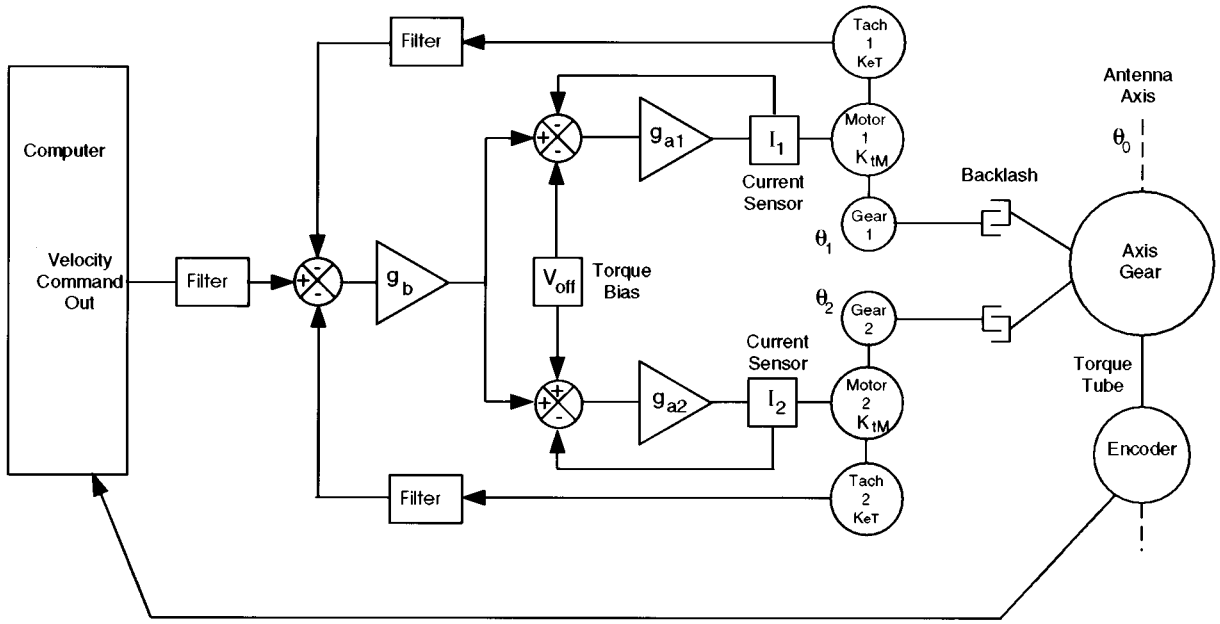

FIG. 6. Schematic of the AST/RO servo system for one axis. Both axes are identical, aside from the servo tuning parameters.

The voltage $V_{\rm off}$ is a constant chosen to provide a torque offset between the two motors:

$$V_{\rm off} \approx 0.2 T_M/(K_{tM} g_a) = 0.9 \text{ V}. \tag{3.18}$$

The combined voltage is input to the amplifier, and the motor connected to the amplifier will produce a torque

$$T_1 = K_{tM} g_{a1} V_{a1} - T_{fM}. \tag{3.19}$$

Equations (3.16), (3.17), and (3.18), and the corresponding equations for motor 2 (with the subscripts 2 and 1 interchanged), along with Eqs. (3.1), (3.2), and (3.3), describe a tracking servo. The gains g_p, g_v, and g_d must be chosen to ensure stable operation.

The electronics shown in Fig. 6 (except for the computer and GMTB sets), plus interface logic, fuses, diagnostic meters, and manual controls are implemented in a single 10 in. high, standard 19 in. rack chassis, the ''drive box.'' The drive boxes for azimuth and elevation are interchangeable. Three boxes were fabricated; one is a plug-compatible spare.

B. Encoders

A shaft encoder is used on each axis, to provide position information to the control computer which is used in the servo loop. Design criteria for the encoders are:

(1) one arcsecond or better resolution (21 bits);
(2) readout is absolute;
(3) the assembled encoder is sufficiently rugged to remain mounted and aligned during shipment;
(4) the operating temperature is between $+40$ and -70 °C;
(5) encoders are identical for both azimuth and elevation axes;
(6) 120 mm or larger hole through center.

While there are commercially manufactured encoders which satisfy these requirements, their price is an order of magnitude more than was allowed by the project budget. Encoders were therefore made in the instrument shop at Bell Laboratories, using Inductosyn™ steel transducer plates, commercial preamplifiers, and one fully constrained 287-mm-diam bearing per encoder. A mounting plate of magnetic stainless steel was machined with pockets for lightening and for mounting the preamplifiers and miniature ''D'' connectors. One of the transducer plates was screwed to this mounting plate, aligned concentric with its outer diameter within 5 μm, and the wires connected. The other transducer plate was mounted to the rotating part of the large-diameter bearing with a shim plate machined to the appropriate thickness, and then aligned concentric to that bearing. The bearing was then screwed to the stainless mounting plate, and aligned. The resulting encoder consists almost entirely of steel parts, and is quite rugged—in one test, it read out accurately with 23 bits of precision while cold-soaked in a box full of dry ice and repeatedly hit with a hammer. Star-pointing tests on the telescope indicate that the encoder is accurate at the subarcsecond level.

One drawback of this encoder design is the ~ 1 N m starting torque of the encoder bearing. The mounting of the encoders to the telescope axes is heavy and stiff, to provide torques sufficient to drive the encoder with less than an arcsecond of wind-up, while accommodating differences in runout between the encoder bearing and the axis bearing. On the elevation axis, the encoder mounts rigidly onto a hub directly on the elevation shaft, and the outer body of the encoder is prevented from moving by a ball bearing which is spring loaded between a flat plate (the plane of which includes the elevation axis) attached to the encoder body and a parallel flat plate attached to the telescope structure. On the azimuth axis, a torque tube is needed to allow room for the cable wrap. The azimuth encoder is screwed directly to the same structural plate which holds the azimuth bearing, and a 228-mm-diam, 10-mm-thick steel torque tube is mounted to

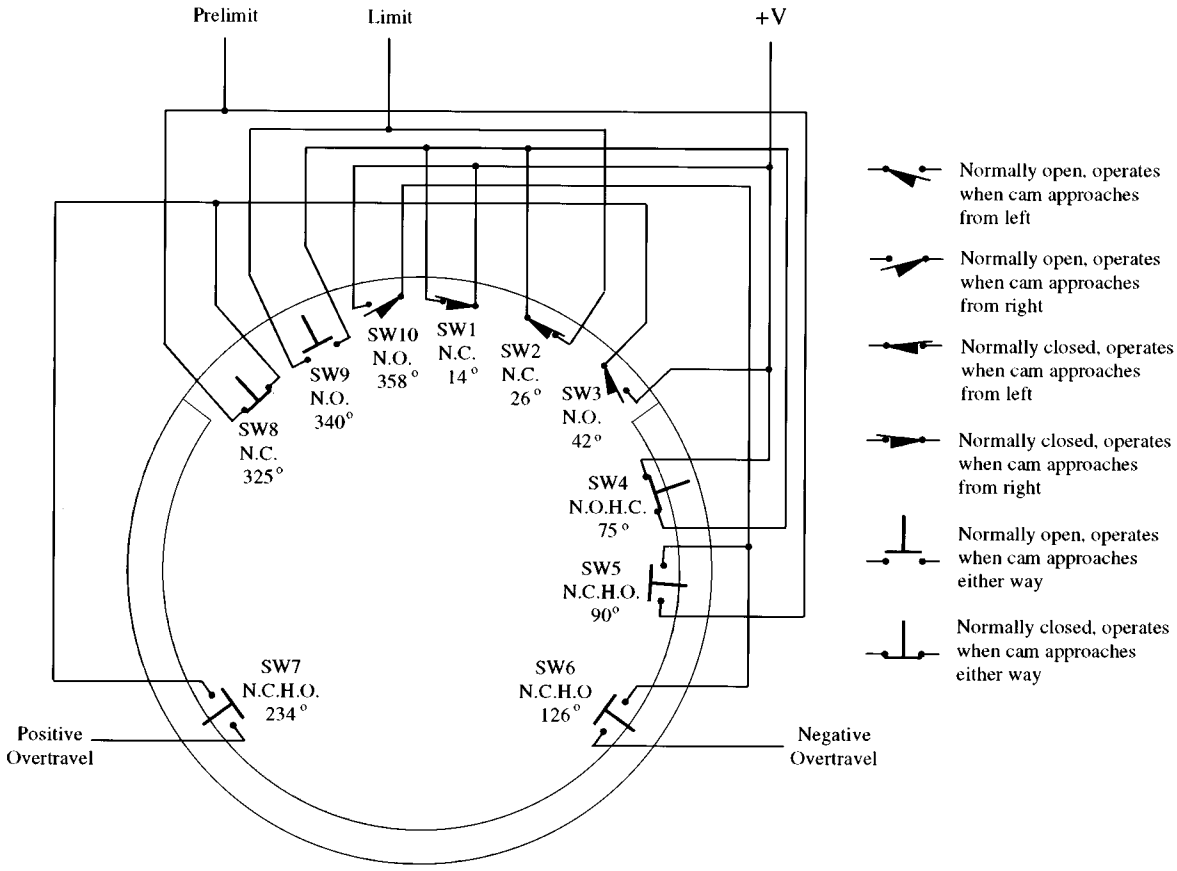

FIG. 7. The limit-switch scheme for AST/RO. The cam is machined into the rotating part of the azimuth bearing mount. The switches do not rotate. The cam and switches are shown for an azimuth of 180°, where the cam edges are presently at 55° and 305°. The angle associated with each switch is the position of the cam edge when the switch is actuated. N.O.—normally open; N.C.—normally closed; H.C.—held closed; H.O.—held open. The wiring illustrates the logic used to derive the limit signals; in practice, each switch is separately interfaced to the computer.

the inner part of the encoder bearing. The torque tube extends upward for a meter, so that the upper end is above the cable wrap, and a lever arm on the end of the tube holds a ball-bearing arrangement similar to the elevation axis.

C. Limit switches

Motion on the azimuth axis is limited by the cable wrap—the cables cannot be wound more than 270° of a turn in either direction (540° total) without damage. Limit switches are needed to prevent telescope motion beyond this range of travel. One complication is that the azimuth axis travel is more than one turn, whereas the encoder is a single-turn type, bounded by 0° and 360°. Turning past 0° to −1° gives a reading of 359°, and turning past 359.99999 to 361° gives a reading of 1°. The limit switches on the azimuth axis must therefore allow more than one turn of travel, and should allow an indication of angles less than 0° and more than 360° (''overtravel''). The overtravel indication should be dependent only on the state of the switches and not on any external memory, so that the system can be turned off and turned back on, or the axes moved with the power off, and the overtravel condition will always be correct. In addition, the limit switches should be robust and must work in conditions of extreme cold. The limit switch scheme should be fail-safe in the sense that no single failure results in damage to the telescope at the limits, and single failures of the limit switches are readily detectable.

The switches chosen are a standard industrial limit switch, unusual only in having a temperature rating of −65 °F. The switch is operated when its lever is overridden by a cam cut into the azimuth structure of the telescope. The switch and lever can be set up so that the switch operates either when the cam approaches from the right only, when the cam approaches from the left only, or when the cam approaches from either direction. Each switch contains both normally closed and normally open contacts, so altogether there are six different modes of operation, as shown in Fig. 7. Suppose the switch is set up to operate when the cam approaches from the left. The lever has a spring return to the center (vertical) position. If the cam overrides the switch from the left, the lever on the switch will rotate clockwise and the switch will operate—the normally open contact will close and the normally closed contact will open. The contacts remain this way until the lever is released by the cam. If the cam overrides the switch from the right, the lever on the switch will rotate counterclockwise, and the lever will remain depressed as long as it is beneath the cam, but the switch will not operate. This property provides the ''memory'' which allows the ensemble of switches to remember how the antenna moved into position, and removes the ambiguity between e.g., 1° and 361°.

TABLE VI. Signals produced by azimuth limit switches.

Signal	Value	Range	Logic
limit	$+V$	$465° > Az > -50°$	$(SW_1+SW_4)\cdot(SW_2+SW_9)$
	open	$Az > 465°$ or $Az < -50°$	
prelimit	open	$450° > Az > -35°$	$SW_3\cdot SW_8+SW_{10}\cdot SW_5$
	$+V$	$Az > 450$ or $Az < -35°$	
positive overtravel	open	$Az < 359°$	$SW_3\cdot SW_7$
	$+V$	$Az > 359°$	
negative overtravel	open	$Az > 1°$	$SW_{10}\cdot SW_6$
	$+V$	$Az < 1°$	

Figure 7 shows the setup and wiring of the azimuth switches. The cam position is shown for an azimuth of 180°. The cam has an open sector of 110° in which the switch levers are not depressed, and a closed sector of 250° in which the levers are depressed (in operating or nonoperating orientations). The cam was milled into the 0.9-m-diam steel support of the azimuth bearing. Four signals are produced: limit, prelimit, positive overtravel, and negative overtravel. The types of signal and the range of azimuth over which they are produced are shown in Table VI. Table VII shows how these signals are generated by opening and closing the switches over various ranges of angles. Note that failure of a single switch might result in failure of either the prelimit or limit, but not both.

D. Calibration system

The calibration system measures the gain and offset of the receiver chain, and the atmospheric emission. From this recorded spectra can be converted from antenna temperature to the equivalent antenna temperature that would be measured by an ideal telescope above the Earth's atmosphere. The calibration system is also used as a chopped source when tuning the receiver for minimum noise temperature.

The calibration system is suspended underneath the azimuth structure above the receiver table, as seen in Fig. 1. Three blackbody calibration loads can be viewed by the receivers: a load at the receiver room ambient temperature and two loads cooled by a closed cycle refrigerator to 40 and 90 K. The ambient temperature load is mounted on a linear actuator and can be moved to block the beam from the sky. The cooled loads are in a Dewar to the side of the beam coming into the Coudé room and are switched into the beam by flat chopper mirrors.

The loads are made from precast Eccosorb CR-110 machined into wedge shaped strips and glued together with Eccosorb CR-110 resin. The back of the load is aluminum, which provides the thermal conducting path to the refrigerator. Eccosorb CR-110 has low absorption but also low surface reflection. Because of this, the loads are relatively thick: 3 cm from front to back. This guarantees that at low temperature and low frequency, when the Eccosorb attenuation decreases, the absorption of $\lambda 1.2$ mm radiation exceeds 0.99.

The measured blackbody temperatures of the cooled calibration loads is not as low as expected. (Load blackbody temperatures where measured by comparing them to a load soaked in liquid nitrogen and assume that the receiver output power was linear in antenna temperature.) The load on the 40 K refrigerator stage has a blackbody temperature of about 100 K and the load on the 90 K stage has a 140 K blackbody temperature. This is due to infrared radiation warming the surface of the loads, which have relatively poor thermal con-

TABLE VII. Azimuth limit switch truth table. O=open, I=closed, 0 indicates open circuit, +indicates+V.

Azimuth angle range	Switch										Signal			
	1	2	3	4	5	6	7	8	9	10	limit	prelimit	+O.T.	−O.T.
<-50	O	I	O	O	I	I	O	O	I	I	0	+	0	+
$-50,-35$	O	I	O	I	I	I	O	O	I	I	+	+	0	+
$-35,-1$	O	I	O	I	O	I	O	O	I	I	+	0	0	+
$-1,+1$	O	I	O	I	O	I	I	O	I	I	+	0	0	+
$+1,90$	O	I	O	I	O	O	I	O	I	I	+	0	0	0
90,105	O	I	O	I	O	O	I	I	I	I	+	0	0	0
105,109	O	I	O	I	O	O	I	I	O	I	+	0	0	0
109,123	O	I	O	I	O	O	O	I	O	I	+	0	0	0
123,139	O	I	O	I	O	O	O	I	O	O	+	0	0	0
139,200	I	I	O	I	O	O	O	I	O	O	+	0	0	0
200,215	I	I	O	O	O	O	O	O	O	O	+	0	0	0
215,251	I	I	O	O	I	O	O	O	I	O	+	0	0	0
251,261	I	I	O	O	I	I	O	O	I	O	+	0	0	0
261,277	I	O	O	O	I	I	O	O	I	O	+	0	0	0
277,310	I	O	I	O	I	I	O	O	I	O	+	0	0	0
310,325	I	O	I	I	I	I	O	O	I	O	+	0	0	0
325,359	I	O	I	I	O	I	O	O	I	O	+	0	0	0
359,361	I	O	I	I	O	I	I	O	I	O	+	0	+	0
361,450	I	O	I	I	O	O	I	O	I	O	+	0	+	0
450,465	I	O	I	I	O	O	I	I	I	O	+	+	+	0
>465	I	O	I	I	O	O	I	I	O	O	0	+	+	0

ductivity. The radiation temperatures of the loads are therefore calibrated manually about once a month against a load immersed in liquid nitrogen, and thermometers on the loads are monitored during observations. This calibration system has worked well in practice, giving reproducible results at the 5% level on repeatative measurements of standard astronomical sources over the course of more than a year.

IV. OPERATIONAL STATUS

The AST/RO telescope was fabricated between 1990 and 1992 at Bell Laboratories, Crawford Hill, NJ, and at the Scientific Instrument Facility at Boston University. In 1993 and 1994, it was installed at a test site in Boston and used for observational tests.[1] In August 1994, this entire working observatory was packed into crates and shipped. Unfortunately, the truck carrying all the equipment was involved in a serious accident. Some of the parts which had been critically positioned in the shop during telescope assembly, such as the encoders, were knocked out of position. When mounted on the AST/RO building at the Pole, the telescope can be enclosed in a retractable cloth and aluminum ''baby-buggy'' cover. This sheltered working environment allowed an unplanned partial disassembly and realignment of the critical components, demonstrating that even delicate mechanical work can be accomplished on the Polar plateau.

The operational telescope meets all design specifications for observations at 600 μm wavelength, except for pointing errors. Operations at shorter wavelengths are planned but have not yet been undertaken. The pointing model and pointing techniques are still under development; the largest remaining problem is $\sim$20 arc sec variations in the tilt of the telescope pier. The following error of the drive system is less than 1 arc sec. The main beam efficiency, which relates the power scale at the receiver to the power scale within the main beam (the product of η_l and η_f in the notation of Ulich and Haas),[12] exceeds 80% at wavelengths between 1.3 mm and 600 μm.

Currently, there are four heterodyne receivers mounted on an optical table suspended from the telescope structure in the spacious, warm Coudé room:

(1) a 230 GHz SIS receiver, 500 K SSB noise temperature;[13]
(2) a 460–500 GHz Schottky-barrier diode receiver, 950 K DSB (this receiver will work without a liquid Helium supply);[14]
(3) a 492 GHz SIS waveguide receiver, 340 K DSB with the current SIS junction;[15]
(4) a 492 GHz SIS quasioptical receiver, 170 K DSB.[16,17]

The laboratory space under the telescope holds three racks of electronics, including two 1.2-GHz wide acousto-optical spectrometers and one high-resolution acousto-optical spectrometer,[18] cryogenic equipment, laboratory benches, and storage for tools.

The first observations from the South Pole were made in January 1995. Figure 8 shows a spectrum of the 492 GHz line of neutral atomic carbon toward the Galactic Center molecular cloud Sagittarius A taken by AST/RO. As of January 1996, AST/RO completed a year of operations. No significant equipment problems occurred. Over 110 000 raw spectra were obtained, including maps of strips through the galactic plane in the 492 GHz line of CI, and detection of some very weak lines (0.2 K km s^{-1}) from the Magellanic clouds.

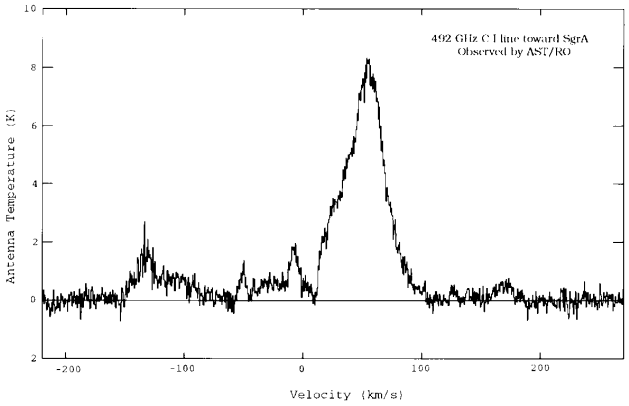

FIG. 8. The 492 GHz line of neutral atomic carbon, in the direction of the Galactic Center molecular cloud Sagittarius A, taken by the AST/RO telescope from the South Pole.

ACKNOWLEDGMENTS

The authors would like to thank Dennis Mumma, Maureen Savage, and Edgar Castro for their work on the drive system. We thank Joe Rottman for the design of the AST/RO building and pier, and John Bally for the design of the Coudé room optical table supports. We thank Robert W. Wilson, John Bally, and Dennis Mumma for discussions on the design of the antenna. We thank the staff of the Boston University Scientific Instrument Facility and the staff of the Bell Laboratories Crawford Hill shop, especially George Pisiello, Al Smith, and Karl Schwarz. They also thank Simon Balm and Adair Lane for help with telescope assembly. This research was supported in part by the National Science Foundation (NSF) under Grant No. OPP88-18384 and under a cooperative agreement with the Center for Astrophysical Research in Antarctica (CARA), Grant No. NSF OPP89-20223. CARA is an NSF Science and Technology Center.

[1] A. A. Stark, A. P. Lane, S. Balm, M. Rumitz, T. Bania, R. Chamberlin, M. Huang, J. Ingalls, J. Jackson, E. Castro, G. Engargiola, K.-Y. Lo, J. Bally, R. W. Wilson, G. Wright, D. Mumma, R. Schieder, J. Stutzki, and J. Staguhn, Antarctic J. U. S. **XXIX**, 344 (1994).
[2] AST/RO is the result of a successful proposal to the United States National Science Foundation by A. A. Stark, J. Bally, and R. W. Wilson of Bell Laboratories, T. M. Bania and A. P. Lane of Boston University, and K.-Y. Lo of the University of Illinois.
[3] J. Bally, in *Astrophysics in Antarctica*, edited by D. J. Mullan, M. A. Pomerantz, and T. Stanev (AIP, New York, 1989), p. 100.
[4] R. A. Chamberlin, A. P. Lane, and A. A. Stark, Astrophys. J. **476**, 428 (1997).
[5] W. Schwerdtfeger, *Weather and Climate of the Antarctic* (Elsevier, New York, 1984), pp. 26–62.
[6] T. S. Chu, IEEE Trans. Antennas Propag. **AP-31**, 614 (1983).
[7] C. Dragone, IEEE Trans. Antennas Propag. **AP-30**, 331 (1982).
[8] D. J. Schroeder, *Astronomical Optics* (Academic, San Diego, 1987), p. 101.
[9] P. F. Goldsmith, in *Infrared and Millimeter Waves*, edited by K. J. Button (Academic, New York, 1982), p. 277.

[10] Fabricated by Dornier GmbH, Friedrichshafen, Germany.
[11] R. N. Bracewell, *Fourier Transform and Its Applications* (McGraw-Hill, New York, 1965), pp. 219–240.
[12] B. L. Ulich and R. W. Haas, Astrophys. J. Suppl. Series **30**, 247 (1976).
[13] This receiver was made in 1989 at Bell Laboratories by J. Bally.
[14] Made by Radiometer Physics, GmbH, Meckenheim, Germany.
[15] Made at the University of Arizona by C. Walker.
[16] G. Engargiola, J. Zmuidzinas, and K.-Y. Lo, Rev. Sci. Instrum. **65**, 1833 (1994).
[17] J. Zmuidzinas and H. G. LeDuc, IEEE Trans. Microwave Theory Tech. **40**, 1797 (1993).
[18] R. Schieder, V. Tolls, and G. Winnewisser, Exp. Astron. **1**, 101 (1989).